arXiv:1612.05217v2 [cond-mat.str-el] 28 Jan 2017

Experimental Approach to the Thermodynamics of the Pure Two-Dimensional Spin-1/2 Triangular Lattice Antiferromagnet in $Ba_8CoNb_6O_{24}$

Y. Cui,[1,*] J. Dai,[1,*] P. Zhou,[1] P. S. Wang,[1] T. R. Li,[1] W. H. Song,[1] L. Ma,[2] Z. Zhang,[3] S. Y. Li,[3,4] G. M. Luke,[5,6] B. Normand,[7] T. Xiang,[8,9] and W. Yu[1,10,†]

[1]*Department of Physics and Beijing Key Laboratory of Opto-electronic Functional Materials & Micro-nano Devices, Renmin University of China, Beijing, 100872, China*
[2]*High Magnetic Field Laboratory, Chinese Academy of Sciences, Hefei 230031, China*
[3]*State Key Laboratory of Surface Physics and Laboratory of Advanced Materials, Department of Physics, Fudan University, Shanghai 200433, China*
[4]*Collaborative Innovation Center of Advanced Microstructures, Nanjing 210093, China*
[5]*Department of Physics and Astronomy, McMaster University, Hamilton L8S 4M1, Canada*
[6]*Canadian Institute for Advanced Research, Toronto M5G 1Z8, Canada*
[7]*Laboratory for Neutron Scattering and Imaging, Paul Scherrer Institute, CH-5232 Villigen PSI, Switzerland*
[8]*Institute of Physics, Chinese Academy of Sciences, Beijing 100190, China*
[9]*Collaborative Innovation Center of Quantum Matter, Beijing 100190, China*
[10]*Department of Physics and Astronomy, Shanghai Jiaotong University, Shanghai 200240, China and Collaborative Innovation Center of Advanced Microstructures, Nanjing 210093, China*

Frustrated quantum magnets pose well-defined questions concerning quantum fluctuation effects and the nature of the many-body wavefunction, which challenge theory, numerics, experiment and materials synthesis. The $S = 1/2$ triangular-lattice antiferromagnet (TLAF) presents a case where classical order is strongly suppressed by quantum fluctuations, leading to extensive renormalization of physical properties at all energy scales. However, purely two-dimensional (2D) models are difficult to realise in the 3D world and their physics is controlled by the Mermin-Wagner theorem, which describes the dominant effects of additional thermal fluctuations. Here we report the magnetic properties $Ba_8CoNb_6O_{24}$, whose Co^{2+} ions have an effective spin 1/2 and construct a regular TLAF with very large interlayer spacing. We find no magnetic ordering down to 0.028 K, strong low-energy spin fluctuations in qualitative agreement with theoretical analysis and a diverging correlation length, all indicating a Mermin-Wagner trend towards zero-temperature ordering in this ideal 2D system.

The Mermin-Wagner theorem [1] describes the combined effects of quantum and thermal fluctuations in the restricted phase space of low-dimensional systems, and dictates that in 2D a continuous symmetry can be broken, allowing a finite order parameter, only at exactly zero temperature. In practice, most experimental systems are subject to a weak 3D coupling which stabilizes their semiclassical order, and so examples of "Mermin-Wagner order," meaning incipient order as $T \to 0$, are rare.

The challenge of frustrated quantum magnetism is to characterize the effects of quantum fluctuations in dimensions greater than 1. While the $S = 1/2$ square-lattice antiferromagnet (SLAF) with Heisenberg interactions has clear magnetic order with a suppressed moment ($m_s \simeq 0.61 m_0$, where m_0 is the full moment for $S = 1/2$) and the kagome-lattice AF has no order at all, the TLAF lies close to the boundary where the frustration is sufficient to destroy m_s, leading to a range of exotic proposals [2–5]. Subsequent studies have demonstrated that the ground state of the Heisenberg TLAF does have a finite semiclassical order, in a noncollinear 120° structure [6, 7], with a best estimate for m_s of $0.41 m_0$ [8]. However, the thermodynamic properties of the TLAF have remained as a long-standing conundrum due to the inadequacy of theoretical approximations, the limitations of numerical approaches (including small system sizes in exact diagonalization, the minus-sign problem in quantum Monte Carlo and the 1D restriction on density-matrix renormalization-group methods) and the absence of pure 2D systems for experimental investigation. A full understanding of the TLAF would also aid the understanding of other novel quantum states, most notably spin liquids [9], unconventional superconductors [10] and systems with complex magnetic order [11], in all of which geometric frustration has an essential role.

A number of spin-1/2 TLAF compounds has been synthesized recently [12, 13]. Of most interest are the materials $Ba_3CoSb_2O_9$ and $Ba_3CoNb_2O_9$, which have perfectly regular lattices of Co^{2+} ions and preservation of inversion symmetry close to the plane, so that Dzyaloshinskii-Moriya (DM) interactions are too small to break the continuous symmetry [14–18]. It is found that these systems are close to a pure Heisenberg interaction, albeit with a weak exchange anisotropy ($J_x = J_y \neq J_z$). Magnetic order occurs at finite temperatures due to weak interplane coupling, which makes the Mermin-Wagner theorem inapplicable. The rich variety of competing magnetically ordered phases at finite applied magnetic

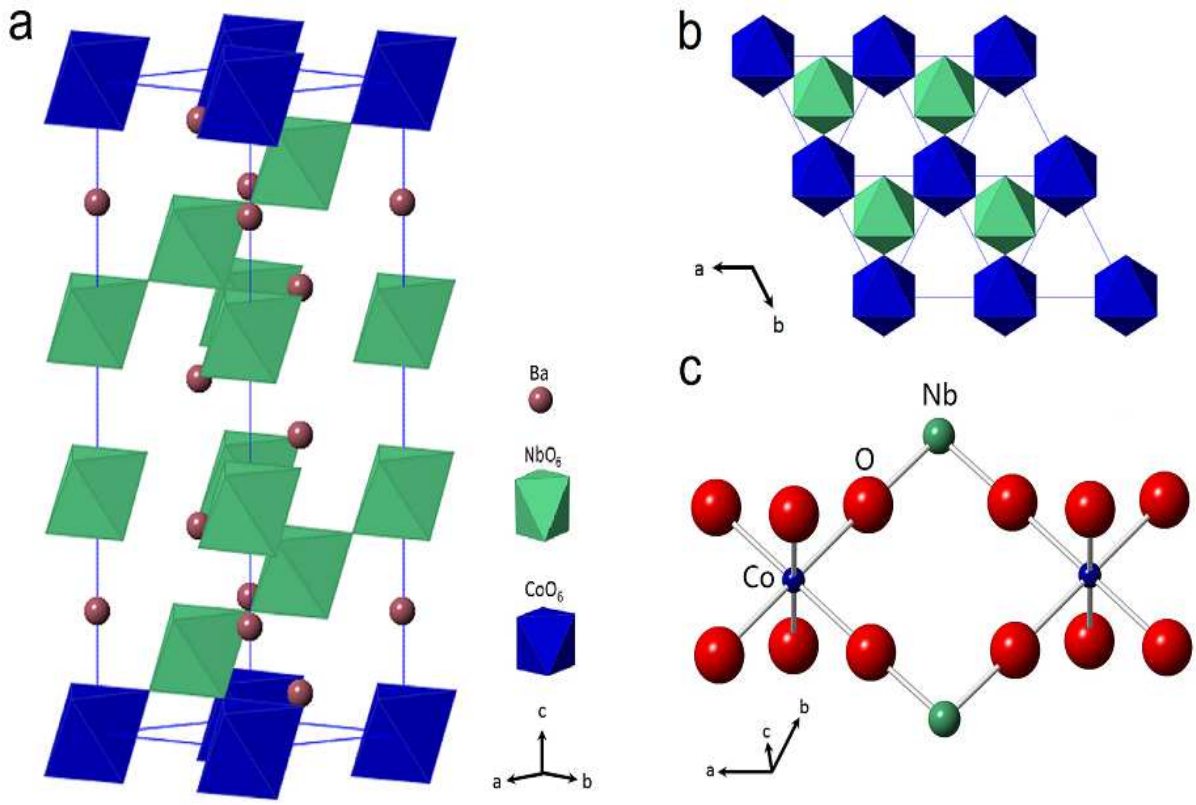

FIG. 1: **Lattice structure of $Ba_8CoNb_6O_{24}$.** (a) The triangular-lattice planes formed from the CoO_6 units are separated by many nonmagnetic units, specifically 8 Ba^{2+} and 6 NbO_6 layers. (b) A plane of CoO_6 octahedra, showing their triangular-lattice configuration and the neighbouring, corner-sharing NbO_6 octahedra which mediate the antiferromagnetic interactions. (c) Local bonding geometry of neighbouring Co^{2+}, Nb^{5+} and O^{2-} sites.

fields [11] provides evidence of the expected frustration effects. Available theoretical approaches [19–23] suggest the presence of weakly dispersive excitations, which have not as yet been observed but whose effects on the thermodynamic properties of the TLAF lie beyond the predictions of the nonlinear-σ model [23–25].

Here we report an experimental approach to the thermodynamic properties of the purely 2D, spin-1/2 TLAF close to the Heisenberg point, which we make by studying the dielectric compound $Ba_8CoNb_6O_{24}$. This system has Co^{2+} triangular layers separated by a very large interlayer spacing, $c \simeq 18.9$ Å. By combining magnetization, g-factor, susceptibility, specific-heat and ^{93}Nb nuclear quadrupole resonance (NQR) measurements down to temperatures of 0.028 K, we reveal that i) the system has an effective spin-1/2 with a nearest-neighbour antiferromagnetic exchange coupling $J \simeq 1.3$ K, ii) there is no spontaneous magnetization down to 0.028 K under zero field but a steeply increasing correlation length upon cooling and iii) the low-temperature susceptibility and specific heat provide a qualitative validation of high-temperature series-expansion (HTSE) and reconstructed Schwinger-boson mean-field (RSBMF) approaches to the TLAF, but quantitative differences remain at the lowest temperatures. (ii) may be the first experimental illustration of the textbook Mermin-Wagner theorem concerning zero-temperature magnetic ordering in a 2D system. (iii) shows anomalously low energy scales and discrepancies from theory which lie in sharp contrast to the properties of the SLAF. Thus $Ba_8CoNb_6O_{24}$ constitutes a model system for characterizing the interplay of geometrical frustration, quantum and thermal fluctuations.

Material

Polycrystalline $Ba_8CoNb_6O_{24}$ samples were synthesized by a solid-state reaction method [26]. The material crystallizes in the space group $P\bar{3}m1$, illustrated in Fig. 1a. Co^{2+} ions in corner-shared CoO_6 octahedra construct perfect layers of regular triangular lattices (Fig. 1b), with neighbouring Co^{2+} planes separated by eight Ba^{2+} and six NbO_6 layers. The lattice parameters [26] are $a = 5.789813$ Å, almost identical to that of $Ba_3CoNb_2O_9$ ($a = 5.7737$ Å), but $c = 18.89355$ Å, which is approximately three times longer.

It is necessary first to establish the effective spin of the Co^{2+} ions in $Ba_8CoNb_6O_{24}$. Figure 2a shows the magnetization, M, as a function of field at a fixed temperature $T = 0.46$ K. M increases rapidly and linearly

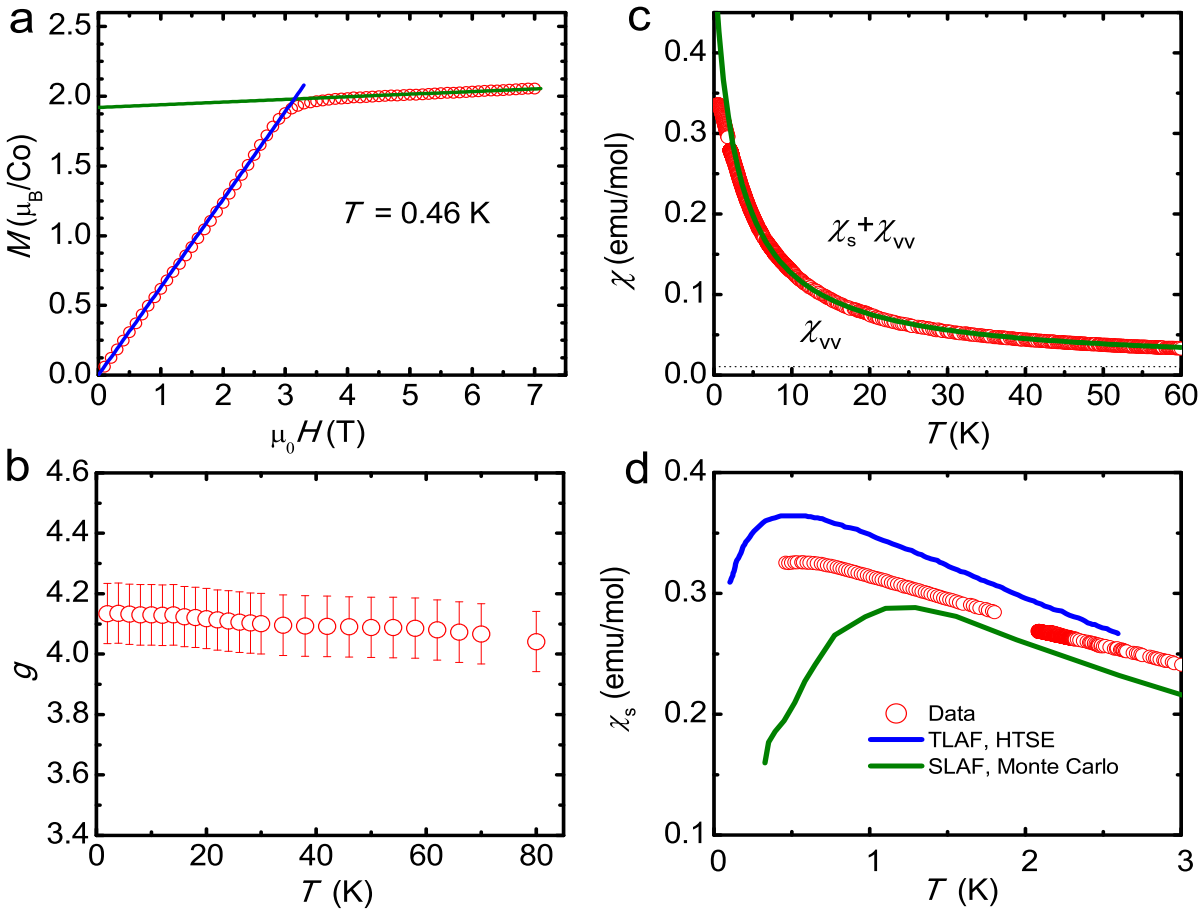

FIG. 2: **Magnetic properties of $Ba_8CoNb_6O_{24}$.** (a) Magnetization, M; blue and green straight lines represent linear-H fits to the low- and high-field data, whose origins lie respectively in spin and orbital contributions. (b) g-factor as a function of temperature. (c) dc susceptibility measured under a field of 0.01 T. χ_{vv} is the constant orbital contribution determined from M. The solid green line is a fit to a Curie-Weiss form, with an offset of χ_{vv}. (d) Enlarged view of the low-temperature spin susceptibility: the blue line shows HTSE results for the Heisenberg TLAF, adapted from Ref. [24]; the green line shows Monte Carlo results for the Heisenberg SLAF, adapted from Ref. [30]. Both fits use the parameters $J = 1.3$ K and $g = 4.13$.

up to a field $H_S = 3.12 \pm 0.04$ T, beyond which a weak linear increase is also observable (the Van Vleck orbital contribution [17], $\chi_{vv} \simeq 0.019\mu_B$/Co/T, or 0.0106 emu/mol). H_S is the saturation field required to polarize fully the magnetic moment of Co^{2+}, as also measured for $Ba_3CoSb_2O_9$ [14–16] and $Ba_3CoNb_2O_9$ [17, 18]. The saturation moment of the Co^{2+} ions deduced from Fig. 2a is $m_s = 1.92 \pm 0.1\mu_B$. Measurements of the g-factor at different temperatures, shown in Fig. 2b, approach a constant value $g = 4.13 \pm 0.1$ below 20 K. The effective spin is therefore $m_s/g\mu_B \simeq 0.464$, which suggests a spin-1/2 state for Co^{2+}. This is consistent with the crystal-field analysis for Co^{2+} in an octahedral environment [14, 27], where a Kramers doublet is formed due to strong spin-orbit coupling, leading to an effective spin-1/2 with a large g-factor at low temperatures.

The magnetic exchange coupling can be estimated from the same data. From the corner-sharing geometry of neighbouring CoO_6 and NbO_6 octahedra, the dominant magnetic interactions between in-plane Co^{2+} spins occur by Co^{2+}-O^{2-}-O^{2-}-Co^{2+} and Co^{2+}-O^{2-}-Nb^{5+}-O^{2-}-Co^{2+} superexchange couplings (Fig. 1c [17]); the very long paths make the interaction strength extremely sensitive to geometrical details and preclude all but nearest-neighbour couplings. For the effective $S = 1/2$ Co^{2+} ions one expects an XXZ spin model of the form $H = \sum_{\langle ij \rangle} J_x(S_i^x S_j^x + S_i^y S_j^y) + J_z S_i^z S_j^z$, where $\langle ij \rangle$ denotes nearest-neighbour Co^{2+} spins [14–18]. In $Ba_3CoSb_2O_9$, the exchange coupling is close to isotropic (Heisenberg), with $J_x = J_y \approx J_z \approx 18.2$ K [14–16]. In $Ba_3CoNb_2O_9$, double magnetic transitions at 1.36 K and 1.10 K in zero field are consistent with a weak easy-axis anisotropy, $J_z > J_x$ [17, 18, 28, 29]. Because $Ba_8CoNb_6O_{24}$ and $Ba_3CoNb_2O_9$ have an almost identical planar structure, very similar exchange couplings are expected: using the result $4.5J = g\mu_B H_S$ for the Heisenberg TLAF at $T = 0$ [11], from Fig. 2a we estimate that $J = 1.3 \pm 0.1$ K for $Ba_8CoNb_6O_{24}$. We comment that this procedure may

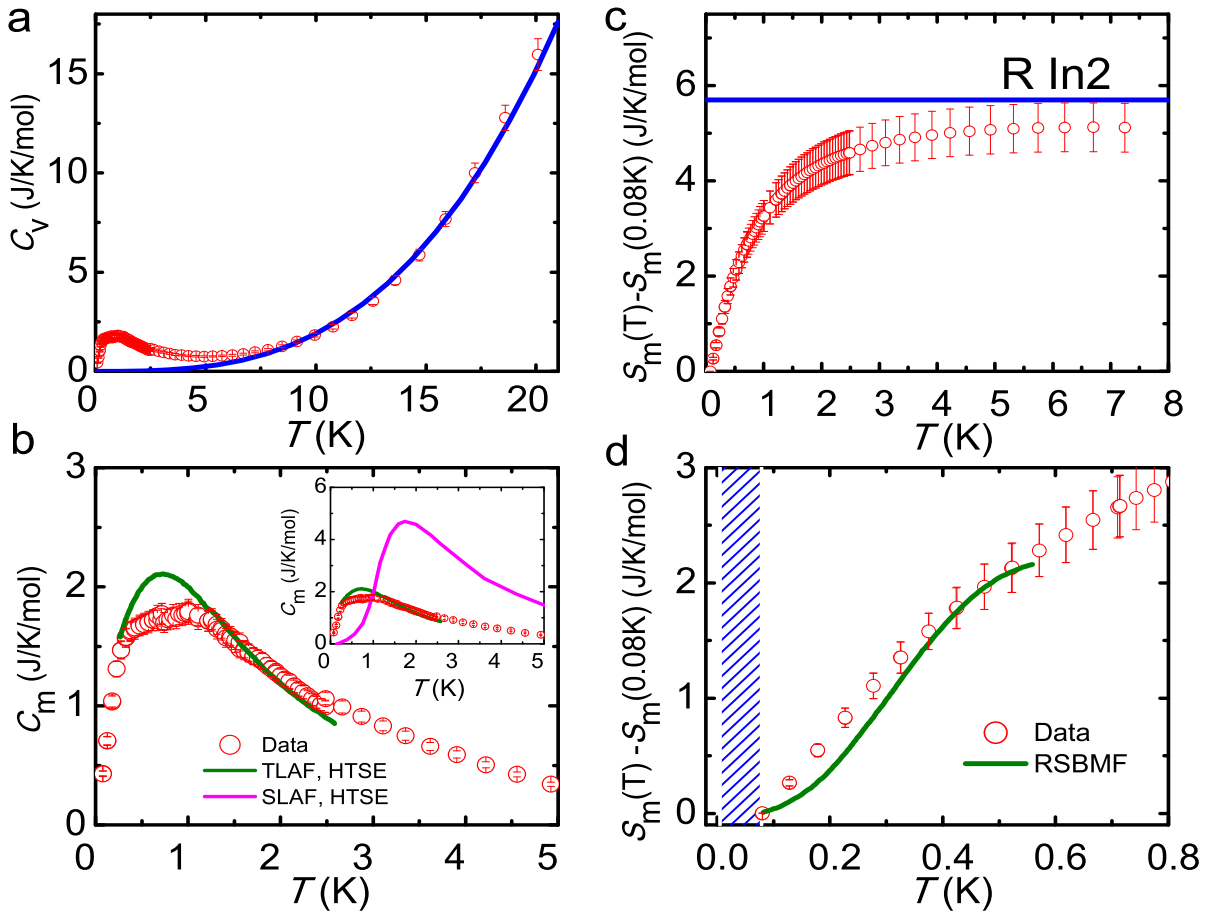

FIG. 3: **Specific heat and entropy analysis.** (a) Specific heat at zero field. The solid line is a fit to $C_v = aT^3$. (b) Enlarged view of the low-temperature magnetic specific heat, C_m, after subtracting the phonon contribution. The green solid line is the HTSE result for the Heisenberg TLAF, adapted from Ref. [24] with $J = 1.3$ K. Inset: TLAF $C_m(T)$ data from the main panel compared with the HTSE result for the Heisenberg SLAF, adapted from Ref. [32], for the same value $J = 1.3$ K. (c) Magnetic entropy, $S_m(T)$, obtained by integrating the specific-heat data above 0.08 K. The solid line shows the high-temperature limit, $S_m(\infty) = \mathrm{R}\ln(2S+1)$ in a spin-S system, for $S = 1/2$. (d) Enlarged view of $S_m(T)$ at low temperature, showing the comparison with the RSBMF approach (see text), adapted from Ref. [23] with $J = 1.3$ K. Blue shading represents the temperature region excluded from our analysis.

underestimate J by a small amount, because our measurement of H_S is not made at zero temperature, but this effect is included within the error bar. In the absence of single crystals we do not speculate on the anisotropy of the exchange couplings in $Ba_8CoNb_6O_{24}$, but from the properties of $Ba_3CoNb_2O_9$ and $Ba_3CoSb_2O_9$ one expects to be close to the Heisenberg model ($J_x \simeq J_z$).

Thermodynamic Properties

Turning to thermodynamic properties, the dc susceptibility, $\chi(T)$, of the sample, measured under a field of 0.01 T, is shown in Fig. 2c. From 20 K down to 1 K, $\chi(T)$ increases upon cooling and can be separated into the two contributions $\chi(T) = \chi_{vv} + \chi_s(T)$. $\chi_s(T)$ follows a Curie-Weiss (CW) form, $\chi_s(T) = a/(T + \theta)$, which represents the average contribution of the coupled Co^{2+} spins and returns a Weiss constant $\theta \approx 3.5 \pm 0.5$ K. At low temperatures, $\chi_s(T)$ is expected to fall below the CW form when $T < J$ and the spins become correlated (Fig. 2c). For comparison, in Fig. 2d we show $\chi_s(T)$ obtained by HTSE on the Heisenberg TLAF, adapted from Ref. [24] by using the parameters $J = 1.3$ K and $g = 4.13$ deduced from M (Fig. 2a).

At the qualitative level, the HTSE fit is completely consistent with our data, in particular the fact that the peak in $\chi_s(T)$ occurs at the anomalously low temperature $T \approx 0.4J$; this can be contrasted with the behaviour of the unfrustrated SLAF (Fig. 2d [30]), where the peak appears at $T \approx J$. Quantitatively, the HTSE fit lies above our data by approximately 10%, and we comment that a better fit would be obtained with a value $J \simeq 1.6$ K. However, such a value would make it impossible to fit M (Fig. 2a) without driving g (Fig. 2b) well outside the error bars on our measurement. Because M constitutes

the most direct and accurate access to J in experiment, we continue to be guided by the value it yields. We comment also that the HTSE is by nature an approach from high temperatures, which reaches its limits at the anomalously low temperatures of the χ_s peak in the TLAF, and its use requires careful choice of representative Padé approximants.

Further valuable thermodynamic information is provided by the specific heat, $C_v(T)$, shown in Fig. 3a. The absence of any peak or cusp feature in C_v suggests that magnetic ordering is absent to the lowest temperature we can access. Because C_v falls rapidly from 20 K to 7.5 K, following an exact T^3 behaviour, we use this to subtract the presumed phonon contribution and isolate the magnetic specific heat, $C_m(T)$. This procedure can be followed with a high degree of confidence because the characteristic energy scales of the phonons are manifestly very high compared to the magnon contributions in this system, which peak at 1 K. However, we caution that even very small residual uncertainties may be important in the entropy analysis below, and contribute to the error bars we display. $C_m(T)$, shown in Fig. 3b, confirms the absence of ordering features, is dominated by a broad peak at $T \approx 1.0$ K and below 0.3 K falls rapidly towards $C_m = 0$ with no evidence for an actived form (i.e. for a spin gap). Once again we compare our data with the HTSE result [24] for the Heisenberg TLAF with $J = 1.3$ K, finding a semi-quantitative level of agreement over the available range of the HTSE data (0.3 K $\leq T \leq$ 2.5 K). As for the susceptibility, the peak in $C_m(T)$ lies at a value anomalously low compared with the energy scale of the SLAF, as deduced from QMC [30] and HTSE methods [31, 32] and shown in the inset of Fig. 3b; this result reflects directly the effects of frustration in suppressing the overall energy scale of the magnetic excitations [25].

The magnetic entropy, $S_m(T) = \int C_m/T dT$, which we calculate from our $C_m(T)$ data by integrating above 0.08 K, is shown in Fig. 3c. At 7.5 K, we estimate that $S_m(T)$ saturates $90 \pm 10\%$ of its total value, $S_m(\infty) = R \ln 2$ for a spin-1/2 system. Because of the errors accumulated in the integration, including those from the phonon subtraction, we cannot draw any meaningful conclusions about possible missing entropy from this result, other than that it is small. At low temperatures, however, we find that $S_m(T)$ has a very rapid initial increase from $T = 0.08$ K, with 33% of $S_m(\infty)$ recovered by $T = 0.3J$ (Fig. 3d). Here we compare our data to the RSBMF approach [23], a modified Schwinger-boson technique which counts the correct number of physical states and thus is expected to capture the key properties of the TLAF in the low-temperature regime. By comparison with our data, the RSBMF formalism provides quantitatively accurate state-counting for $T > 0.3J$, which we note is near the limit of the authors' claims for its validity. However, the form of $S_m(T)$ at lower temperatures is not well described, a result on which we comment briefly below. Nevertheless, we note for perspective that the type of nonlinear-σ-model approach so effective for the SLAF recovers only 5% of the total entropy at $T = 0.3J$ in the TLAF [24, 33] and therefore appears incapable of providing a suitable account of frustrated systems.

NQR Measurements

To probe both static and low-energy magnetic properties, we present low-temperature ^{93}Nb NQR data. Here we report only the signal with the shortest spin-lattice relaxation time, $^{93}T_1$, which is over three orders of magnitude faster than the other times present and arises in all probability from the Nb sites closest to the Co^{2+} layers (i.e. with strong hyperfine coupling to the Co^{2+} moments). The ^{93}Nb ($I = 9/2$) NQR spectra for excitations between $I_z = \pm 9/2$ and $I_z = \pm 7/2$ are shown in Fig. 4 (a), for temperatures from 0.8 K to 0.028 K and with intensity normalized by the Zeeman factor, $1/T$. At $T = 0.028$ K, the spectrum is well fitted by a Gaussian function (red line), and this fit is applied also to the spectra at 0.2 K, 0.4 K and 0.8 K. Clearly all spectra are centred at the same frequency, $f = 4.212$ MHz, and the echo intensity remains constant with temperature. The absence of any signal loss and of any NQR frequency shift completely excludes any magnetic order down to 0.028 K, consistent with the specific-heat data. Because the ^{93}Nb nucleus is located directly above the centre of one triangle composed of three Co^{2+} ions (Fig. 1b), the static hyperfine field on ^{93}Nb should be finite with an off-diagonal component, if the Co^{2+} moments order with the 120° coplanar pattern [11], and thus it is highly unlikely that magnetic order could be missed by the NQR spectra.

The NQR spin-lattice relaxation rate, $1^{93}/T_1$, shown in Fig. 4b, probes the low-energy spin fluctuations. In general, $1/T_1 = \sum_q A_{hf}(q) \mathrm{Im}\chi^{\pm}(q,\omega)/\omega|_{\omega\to 0}$, where A_{hf} is the hyperfine coupling constant and $\chi^{\pm}(q,\omega)$ the transverse dynamic susceptibility. The fact that $1/^{93}T_1$ is of order 10 s^{-1} indicates very strong hyperfine coupling between ^{93}Nb and the Co^{2+} spins. $1/^{93}T_1$ also contains no evidence for long-range order, although its moderate upturn below 0.2 K indicates an increasing correlation length, precisely as would be expected if the system approaches the zero-temperature magnetic order anticipated by the Mermin-Wagner theorem [1]. To our knowledge, this is the first direct observation of incipient "Mermin-Wagner" order in a purely 2D magnetic system.

Discussion

For a deeper understanding of the anomalous low energy scale observed in the thermodynamic quantities of Fig. 3, we turn to the most sophisticated HTSE [19, 25], self-consistent spin-wave [20, 21] and RSBMF treatments [23] of the Heisenberg TLAF. These demonstrate that the

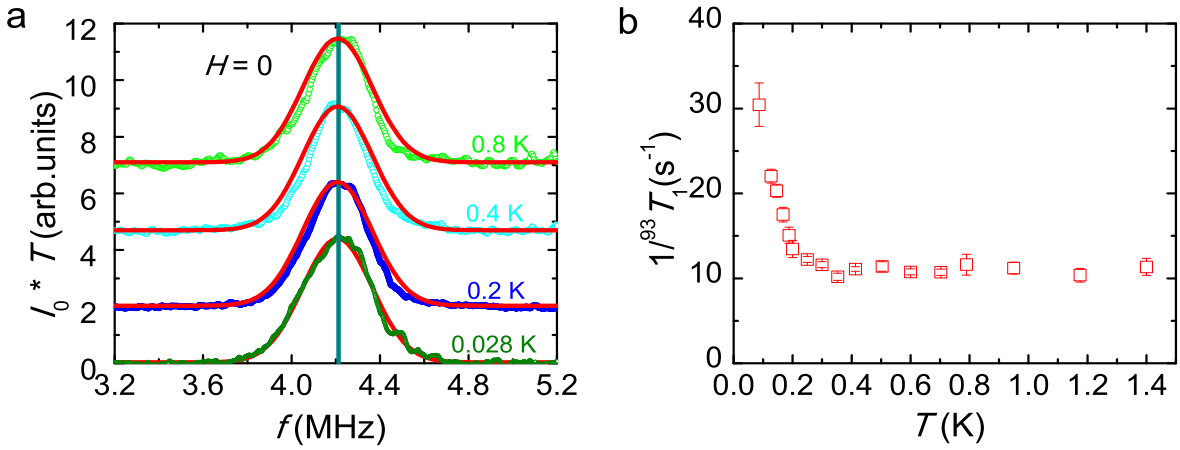

FIG. 4: **NQR measurements of $Ba_8CoNb_6O_{24}$.** (a) Zero-field ^{93}Nb NQR spectra for temperatures from 0.8 K to 0.028 K, with the measured intensity multiplied by T. Red lines represent the Gaussian fit to the spectrum at 0.028 K overlaid on all four datasets. (b) Spin-lattice relaxation rate, $1/^{93}T_1$, as a function of temperature. The upturn below 0.2 K indicates a progessive increase of the correlation length upon cooling.

magnetic excitation band is both extremely flat and unusually low-lying, with strong weight around $E \approx 0.6J$. This is a direct consequence of the strong frustration of the TLAF and stands in sharp contrast to the SLAF, where the bands disperse uniformly up to energies $E \approx 2J$ [34]. The frustration-renormalized energy scale is completely consistent with the temperature-dependence we benchmark in the peak features of $\chi(T)$ and $C_m(T)$. These unusual low-energy excitations of the TLAF have been variously described as "roton-like" or as evidence of fermion deconfinement [19, 20].

To our knowledge, $Ba_8CoNb_6O_{24}$ allows the first direct comparison between theory and a real material for the spin-1/2 Heisenberg TLAF. Small but finite discrepancies do appear at the quantitative level. The HTSE results for $C_m(T)$ (Fig. 3b) appear to overestimate the peak contributions in our data and underestimate those at higher energies. The RSBMF approach appears to underestimate the low-temperature entropy. Both results may be explained if the "roton gap," the effective bandwidth or other features affecting the density of states in the spin spectrum, all of which require a correct accounting for quantum fluctuation effects, are not reproduced perfectly by the theoretical or numerical approaches applied. However, we caution that the mismatch between our data and the theoretical results shown in Figs. 2 and 3 cannot be interpreted unambiguously as evidence for shortcomings in the theories, as it may be caused by small additional terms in the magnetic Hamiltonian, most notably a weakly non-Heisenberg anisotropy in the exchange couplings. We defer a further analysis of this point until single crystals become available.

In summary, we have performed experimental measurements of the thermodynamic and NQR response of a purely 2D TLAF. This model system is realized in the compound $Ba_8CoNb_6O_{24}$, where the very large separation of magnetic layers precludes any 3D coupling. The material illustrates clearly the Mermin-Wagner theorem for a 2D system by the absence of the magnetic ordering down to 0.028 K but a possible zero-temperature order reflected in the increase of $1/T_1$ below 0.2 K. The anomalously low thermodynamic energy scales gauge the strong suppression and flattening of the excitation bands and our measurements benchmark the efficacy of advanced theoretical and numerical approaches in reproducing these frustration-induced properties of the TLAF.

Methods

Polycrystals of $Ba_8CoNb_6O_{24}$ were synthesized by a solid-state reaction method [26]. Magnetization and susceptibility data were measured in a PPMS-VSM for temperatures $T > 2$ K and in a ^{3}He SQUID system for $0.6K < T < 1.8$ K. The temperature-dependent g-factors were obtained by field-sweep ESR at a fixed frequency 9.397 GHz. The specific heat was measured in a PPMS dilution refrigerator (DR), which reached temperatures down to 0.08 K. The ^{93}Nb ($I = 9/2$) NQR signal was detected by the spin-echo technique in a DR system reaching temperatures down to 0.028 K. The spin-lattice relaxation rate, $1/^{93}T_1$, was determined by the inversion-recovery method, and the spin recovery is fit by the standard function $I(t) = I(\infty) - a[4/33e^{-3t/T_1} + 80/143e^{-10t/T_1} + 49/165e^{-21t/T_1} + 16/715e^{-36t/T_1}]$ for $I = 9/2$ spins [35]. The theoretical values for the thermodynamic quantities $\chi(T)$, $C_m(T)$ and $S_m(T)$ were digitized from the cited literature and scaled appropriately.

* These authors contributed equally to this study.

† Electronic address: wqyu˙phy@ruc.edu.cn

[1] Mermin, N. D. & Wagner, H. Absence of Ferromagnetism or Antiferromagnetism in One-or Two-dimensional Isotropic Heisenberg Models. *Phys. Rev. Lett.* **17**, 1133 (1966).

[2] Anderson, P. W. Resonating valence bonds: A new kind of insulator? *Mater. Res. Bull.* **8**, 153 (1973).

[3] Momoi, T. & Suzuki, M. Ground-State Properties and Phase Diagram of the Quantum XXZ Antiferromagnet on a Triangular Lattice. *J. Phys. Soc. Japan* **61**, 3277 (1992).

[4] Chernyshev, A. L. & Zhitomirsky, M. E. Magnon Decay in Noncollinear Quantum Antiferromagnets. *Phys. Rev. Lett.* **97**, 207202 (2006).

[5] Starykh, O. A. Unusual ordered phases of highly frustrated magnets: a review. *Rep. Prog. Phys.* **78**, 052502 (2015).

[6] Bernu, B., Lhuillier, C. & Pierre, L. Signature of Néel Order in Exact Spectra of Quantum Antiferromagnets on Finite Lattices. *Phys. Rev. Lett.* **69**, 2590 (1992).

[7] Capriotti, L., Trumper, A. E. & Sorella, S. Long-Range Néel Order in the Triangular Heisenberg Model. *Phys. Rev. Lett.* **82**, 3899 (1999).

[8] White, S. R. & Chernyshev, A. L. Néel order in square and triangular lattice Heisenberg models. *Phys. Rev. Lett.* **99**, 127004 (2007).

[9] Balents, L. Spin liquids in frustrated magnets. *Nature (London)* **464**, 199 (2010).

[10] Norman, M. R. Unconventional Superconductivity. in *Novel Superfluids, Vol. 2* (ed. Bennemann, K. H. and Ketterson, J. B.) (Oxford University Press, 2014).

[11] Yamamoto, D., Marmorini, G. & Danshita, I. Quantum Phase Diagram of the Triangular-Lattice XXZ Model in a Magnetic Field. *Phys. Rev. Lett.* **112**, 127203 (2014).

[12] Coldea, R., Tennant, D. A., Tsvelik, A. M. & Tylczynski, Z. Experimental Realization of a 2D Fractional Quantum Spin Liquid. *Phys. Rev. Lett.* **86**, 1335 (2001).

[13] Shimizu, Y., Miyagawa, K., Kanoda, K., Maesato, M. & Saito, G. Spin Liquid State in an Organic Mott Insulator with a Triangular Lattice. *Phys. Rev. Lett.* **91**, 107001 (2003).

[14] Shirata, Y., Tanaka, H., Matsuo, A. & Kindo, K. Experimental Realization of a Spin-1/2 Triangular-Lattice Heisenberg Antiferromagnet. *Phys. Rev. Lett.* **108**, 057205 (2012).

[15] Zhou, H. D., Xu, C., Hallas, A. M., Silverstein, H. J., Wiebe, C. R., Umegaki, I., Yan, J. Q., Murphy, T. P., Park, J.-H., Qiu, Y., Copley, J. R. D., Gardner, J. S. & Takano, Y. Successive Phase Transitions and Extended Spin-Excitation Continuum in the $S = 1/2$ Triangular-Lattice Antiferromagnet $Ba_3CoSb_2O_9$. *Phys. Rev. Lett.* **109**, 267206 (2012).

[16] Susuki, T., Kurita, N., Tanaka, T., Nojiri, H., Matsuo, A., Kindo, K. & Tanaka, H. Magnetization Process and Collective Excitations in the $S = 1/2$ Triangular-Lattice Heisenberg Antiferromagnet $Ba_3CoSb_2O_9$. *Phys. Rev. Lett.* **110**, 267201 (2013).

[17] Lee, M., Hwang, J, Choi, E. S., Ma, J., De la Cruz, C. R., Zhu, M., Ke, X., Dun, Z. L. & Zhou, H. D. Series of phase transitions and multiferroicity in the quasi-two-dimensional spin-1/2 triangular-lattice antiferromagnet $Ba_3CoNb_2O_9$. *Phys. Rev. B* **89**, 104420 (2014).

[18] Yokota, K., Kurita, N. & Tanaka, H. Magnetic phase diagram of the $S = 1/2$ triangular-lattice Heisenberg antiferromagnet $Ba_3CoNb_2O_9$. *Phys. Rev. B* **90**, 014403 (2014).

[19] Zheng, W., Fjærestad, J. O., Singh, R. R. P., McKenzie, R. H. & Coldea, R. Anomalous Excitation Spectra of Frustrated Quantum Antiferromagnets. *Phys. Rev. Lett.* **96**, 057201 (2006).

[20] Starykh, O. A., Chubukov, A. V. & Abanov, A. G. Flat spin-wave dispersion in a triangular antiferromagnet. *Phys. Rev. B* **74**, 180403(R) (2006).

[21] Mourigal, M., Fuhrman, W. T., Chernyshev, A. L. & Zhitomirsky, M. E. Dynamical structure factor of the triangular-lattice antiferromagnet. *Phys. Rev. B.* **88**, 094407 (2013).

[22] Chubukov, A. V., Senthil, T., & Sachdev, S. Universal Magnetic Properties of Frustrated Quantum Antiferromagnets in Two Dimensions. *Phys. Rev. Lett.* **72**, 2089 (1994).

[23] Mezio, A., Manuel, L. O., Singh, R. R. P. & Trumper, A. E. Low temperature properties of the triangular-lattice antiferromagnet: a bosonic spinon theory. *N. J. Phys* **14**, 123033 (2012).

[24] Elstner, N., Singh, R. R. P. & Young, A. P. Finite Temperature Properties of the Spin-1/2 Heisenberg Antiferromagnet on the Triangular Lattice. *Phys. Rev. Lett.* **71**, 1629 (1993).

[25] Zheng, W., Fjærestad, J. O., Singh, R. R. P., McKenzie, R. H. & Coldea, R. Excitation spectra of the spin-1/2 triangular-lattice Heisenberg antiferromagnet. *Phys. Rev. B* **74**, 224420 (2006).

[26] Mallinson, P. M., Allix, M. M. B., Claridge, J. B., Ibberson, R. M., Iddles, D. M., Price, T. & and Rosseinsky, M. J. $Ba_8CoNb_6O_{24}$: A d^0 Dielectric Oxide Host Containing Ordered d^7 Cation Layers 1.88 nm Apart. *Angew. Chem.* **117**, 7911 (2005).

[27] Shiba, H., Ueda, Y., Okunishi, K., Kimura, S. & Kindo, K. Exchange Interaction via Crystal-Field Excited States and Its Importance in $CsCoCl_3$. *J. Phys. Soc. Japan* **72**, 2326 (2003).

[28] Matsubara, F. Magnetic Ordering in a Hexagonal Antiferromagnet. *J. Phys. Soc. Japan* **51**, 2424 (1982).

[29] Miyashita, S. & Kawamura, H. Phase Transitions of Anisotropic Heisenberg Antiferromagnets on the Triangular Lattice. *J. Phys. Soc. Japan* **54**, 3385 (1985).

[30] Makivić, M. S. & Ding, H. Q. Two-dimensional spin-1/2 Heisenberg antiferromagnet: A quantum Monte Carlo study. *Phys. Rev. B* **43**, 3562 (1991).

[31] Wang, J. Two-dimensional spin-1/2 Heisenberg antiferromagnet at finite temperature. *Phys. Rev. B* **44**, 2396 (1991).

[32] Bernu, B. & Misguich, G. Specific heat and high-temperature series of lattice models: Interpolation scheme and examples on quantum spin systems in one and two dimensions. *Phys. Rev. B* **63**, 134409 (2001).

[33] Chubukov, A. V., Sachdev, S. & Senthil, T. Universal Magnetic Properties of Frustrated Quantum Antiferromagnets in Two Dimensions. *J. Phys.: Condens. Matter* **6**, 8891 (1994).

[34] Makivić, M. & Jarrell, M. Low-Temperature Dynamics of the 2D Spin-1/2 Heisenberg Antiferromagnet: A Quantum Monte Carlo Study. *Phys. Rev. Lett.* **68**, 1770 (1992).

[35] MacLaughlin, D. E., Williamson, J. D. & Butterworth, J. Nuclear Spin-Lattice Relaxation in Pure and Impure Indium. I. Normal State. *Phys. Rev. B* **4**, 60 (1971).

Acknowledgements
We thank A. Honecker, J. Richter, R. Yu and Y. Zhou for helpful discussions. This Work was supported by the National Science Foundation of China (Grant Nos. 11222433 and 11374364), the Ministry of Science and Technology of China (Grant Nos. 2016YFA0300503 and 2016YFA0300504) and the Fundamental Research Funds for the Central Universities and the Research Funds of Renmin University of China (Grant No. 14XNLF08).

Author contributions
The project was conceived by W.Q.Y. The crystals were grown by J.D. High-temperature ($T > 2.5$ K) susceptibility and specific-heat measurements were made by J.D. DR NQR measurements were performed by Y.C., with assistance from P.Z., P.S.W., T.R.L. and W.H.S. Z.Z. and S.Y.L. made DR specific-heat measurements. L.M. made g-factor measurements. Susceptibility and magnetization measurements in the ^{3}He-SQUID were made by G.M.L. The theoretical framework was provided by B.N. and T.X. Data refinement and figure preparation were performed by Y.C. and W.Q.Y. The text was written by B.N. and W.Q.Y.

Additional information
The authors declare no competing financial interests. Correspondence and requests for materials should be addressed to W.Q.Y. (wqyu_phy@ruc.edu.cn).